WATER RESOURCES RESEARCH, VOL. 49, 115–126, doi:10.1029/2012WR012001, 2013

Ecogeomorphic coevolution of semiarid hillslopes: Emergence of banded and striped vegetation patterns through interaction of biotic and abiotic processes

Patricia M. Saco[1] and Mariano Moreno-de las Heras[1,2]

Received 18 February 2012; revised 9 November 2012; accepted 15 November 2012; published 11 January 2013.

[1] Nonlinear interactions between physical and biological factors give rise to the emergence of remarkable landform-vegetation patterns. Patterns of vegetation and resource redistribution are linked to productivity and carrying capacity of the land. As a consequence, growing concern over ecosystem resilience to perturbations that could lead to irreversible land degradation imposes a pressing need for understanding the processes, nonlinear interactions, and feedbacks, leading to the coevolution of these patterns. For arid and semiarid regions, causes for concern have increased at a rapid pace during the last few decades due to growing anthropic and climatic pressures that have resulted in the degradation of numerous areas worldwide. This paper aims at improving our understanding of the ecogeomorphic evolution of landscape patterns in semiarid areas with a sparse biomass cover through a modeling approach. A coupled vegetation-pattern formation and landform evolution model is used to study the coevolution of vegetation and topography over centennial timescales. Results show that self-organized vegetation patterns strongly depend on feedbacks with coevolving landforms. The resulting patterns depend on the erosion rate and mechanism (dominance of either fluvial or diffusive processes), which are affected by biotic factors. Moreover, results show that ecohydrologic processes leading to banded pattern formation, when coupled with landform processes, can also lead to completely different patterns (stripes of vegetation along drainage lines) that are equally common in semiarid areas. These findings reinforce the importance of analyzing the coevolution of landforms and vegetation to improve our understanding of the patterns and structures found in nature.

Citation: Saco, P. M., and M. Moreno-de las Heras (2013), Ecogeomorphic coevolution of semiarid hillslopes: Emergence of banded and striped vegetation patterns through interaction of biotic and abiotic processes, *Water Resour. Res.*, *49*, doi:10.1029/2012WR012001.

1. Introduction

[2] Ecogeomorphologic systems exhibit highly nonlinear interactions between physical and biological factors [*National Research Council*, 2010; *Wheaton et al.*, 2011] that lead to the emergence of remarkable and intriguing landform-vegetation patterns [*Corenblit and Steiger*, 2009; *Reinhardt et al*., 2010; *Saco and Rodriguez*, 2013]. These self-organizing patterns result from the coevolution of landforms and biota, which makes the understanding and prediction of landscape responses to change highly challenging. Vegetation patterns and resource redistribution are linked to productivity and carrying capacity of the land [*Okin et al.*, 2009; *Ravi et al*., 2010; *Moreno-de las Heras et al*., 2012]. Growing concern over ecosystem resilience to climate and land use perturbations that could result in irreversible degradation imposes a pressing need for research, aiming at elucidating the processes, feedbacks, and dynamics leading to these coevolving patterns. Degradation trends have been linked to feedback effects between biota and erosion processes [*Wilcox et al*., 2003; *Ludwig et al*., 2005; *Boer and Puigdefábregas*, 2005; *Michaelides et al*., 2009], which highlights the importance of the analysis and modeling of coevolving semiarid landform-vegetation systems. Even though during the last decade, some exciting advances have been made in this area [*Baas and Nield*, 2007; *Saco et al*., 2007; *Ravi et al*., 2010; *Yetemen et al*., 2010; *Collins and Bras*, 2010], much more progress is still needed [*National Research Council*, 2010]. This paper aims at improving our understanding of the effect of abiotic (relief, erodibility, and soil diffusion) and biotic factors (protective effect of vegetation on soil) on the processes and feedbacks that lead to different landforms and vegetation patterns in semiarid areas.

[3] Semiarid vegetation patterns emerge from nonlinear plant-water interactions [*Tongway and Ludwig*, 2001; *Rietkerk et al*., 2004; *Meron et al*., 2004; *Scanlon et al*., 2007;

[1]Civil, Surveying and Environmental Engineering, The University of Newcastle, Callaghan, New South Wales, Australia.
[2]Department of Ecology, Faculty of Sciences, University of Alcalá, Alcalá de Henares (Madrid), Spain.

Corresponding author: P. M. Saco, Civil, Surveying and Environmental Engineering, The University of Newcastle, Callaghan, New South Wales, 2308, Australia. (Patricia.Saco@newcastle.edu.au)

0043-1397/13/2012WR012001

Kéfi et al., 2007; *Caylor et al*., 2009; *Franz et al*., 2010] that lead to greater soil moisture availability in vegetation patches due to: (i) absence of the biological soil crusts found in bare areas, and increased infiltration rates induced by roots, soil aggregation, macropores, and/or sediment redistribution [*Belnap et al*., 2005; *Thompson et al*., 2010] and (ii) reduction of soil evaporation by vegetation canopy [*Scholes and Archer*, 1997]. Higher infiltration rates under vegetation give rise to the emergence of a runoff-runon system [*Tongway and Ludwig*, 2001]. Runon infiltrated into vegetated patches can be much higher than direct local rainfall [*Valentin et al*., 1999; *Dunkerley*, 2002; *Wilcox et al*., 2003]. This runoff-runon mechanism generates a positive feedback effect by increasing soil moisture and growth in the vegetated patches [*Valentin et al*., 1999; *Puigdefábregas et al*., 1999; *Wilcox et al*., 2003]. The redistribution of runoff from sources (bare areas) to sinks (vegetation patches) is fundamentally important for the maintenance of hillslope functionality in drylands. Disturbances affecting patch structure and surface water connectivity can lead to severe degradation [*Okin et al*., 2009; *Moreno-de las Heras et al*., 2011a]. Increases in connectivity potentially increase runoff and erosion (particularly in steeper slopes) which can lead to flow concentration and rill development [*Turnbull et al*., 2008; *Mayor et al*., 2008], to a decrease in overall productivity, and to changes in the coevolving vegetation patterns [*Puigdefábregas*, 2005; *Moreno-de las Heras et al*., 2011a, 2011b, 2012].

[4] Most of the recent modeling studies on vegetation pattern emergence in semiarid areas have focused on the incorporation of mechanistic processes to simulate the spatial redistribution of plant biomass and water over a fixed topographic profile [*Borgogno et al*., 2009, and references therein]. Though these studies have provided valuable information on mechanisms for pattern formation, they do not include landform-water-vegetation feedbacks, which can potentially lead to alternative patterns and/or dynamic equilibrium states. As mentioned earlier, field studies show that vegetation patterns are regulated by fluvial source-sink processes that coevolve with landforms (i.e., redistribution of both runoff and sediments) [*Michaelides et al*., 2009; *Wainwright et al*., 2002; *Puigdefábregas*, 2005, and references therein]. For instance, Puigdefábregas and coworkers describe transitions between vegetation patterns for varying rates of sediment redistribution for a semiarid site in southeastern Spain [*Puigdefábregas and Sánchez*, 1996; *Puigdefábregas et al*., 1999; *Puigdefábregas*, 2005]. Significant differences were found between water and soil fluxes measured at varying positions relative to the tussocks stands, with approximately 50% of runoff and sediments produced in bare areas intercepted on the upper portion of the tussocks stands. These studies also report that for low sediment movement rates (i.e., milder slopes) parallel bands of tussocks develop along contour lines, promoting soil moisture availability for plants and storage of sediments. However, for higher erosion rates, rills appear preventing the formation of banded vegetation, increasing redistribution distances and promoting the formation of stripes of vegetation in the slope direction. In what follows, we will refer to vegetation bands to allude to those aligned to contour lines, and vegetation stripes for those found along drainage lines with concentrated flow. Many areas worldwide exhibit similar transitions between banded and striped patterns. It is not uncommon to find these patterns in close proximity or even intermingled. Figure 1 displays examples of Google Earth images showing the proximity of banded and striped vegetation patterns for sites in Niger, Australia, and Mexico.

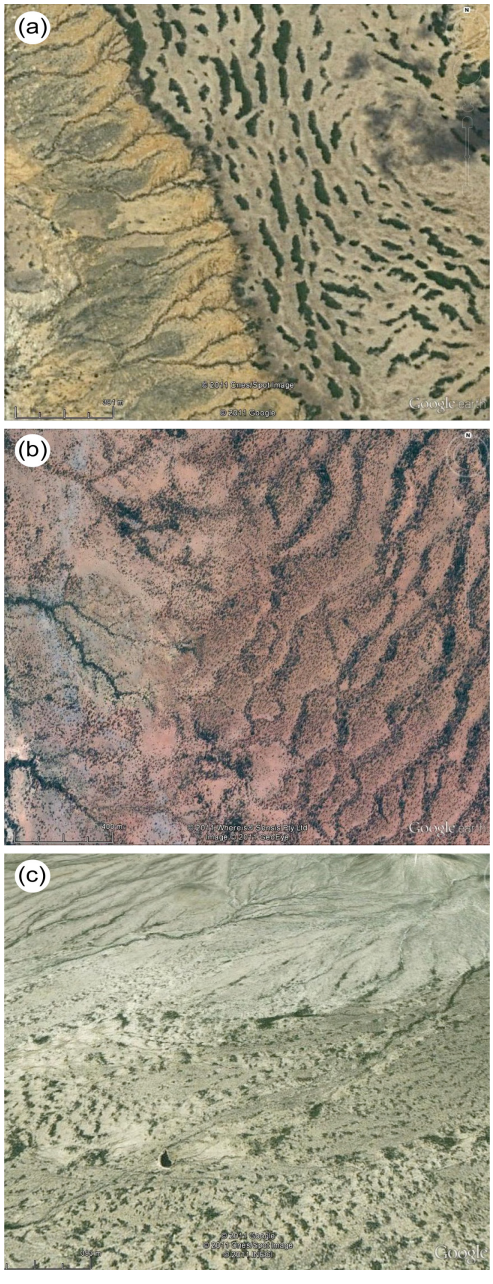

Figure 1. Example of aerial images, obtained from Google Earth, showing banded vegetation patterns in close proximity to vegetation stripes along drainage lines in: (a) Niger (13°50′09.73″N, 2°27′19.97″E), © 2011 Cnes/Spot Image, © 2011 Google; (b) Western Australia (25°31′58.23″S, 115°50′23.27″E), © 2011 Whereis® Sensis Pty Ltd Image © 2011 GeoEye; and (c) México (27°52′33.52″N, 103°47′09.02″W), © 2011 Cnes/Spot Image, © 2011 Google, © 2011 INEGI.

[5] Previous research on modeling vegetation pattern formation on semiarid areas has focused on areas with gentle slopes that give rise to banded or spotted patterns [*Tongway and Ludwig*, 2001; *Rietkerk et al*., 2004; *Meron et al*., 2004; but see *Sánchez and Puigdefábregas*, 1994]. *Saco et al*. [2007] further investigated the interactions between banded vegetation patterns and microtopography in this type of environments. However, as illustrated in Figure 1, other types of vegetation patterns are not uncommon in these areas. Moreover, these studies have not explained why banded vegetation has also been observed in relatively steep areas [*Valentin et al*., 1999], which conditions can lead to the development of banded and striped patterns in close proximity (as shown in Figure 1), and under which conditions one of those patterns will prevail over the other. We address this knowledge gap using a modeling framework to explore how different environmental conditions, which affect the dominance of various erosion processes (diffusive versus fluvial), and the feedbacks between vegetation and erosion, lead to the appearance of different types of patterns. In addition, we also investigate the influence of erodibility reduction induced by the positive effect of plants, which enhance soil quality via organic material and litter [*Zhang*, 1994; *Cerdà*, 1998] and increase of soil aggregation [*Cerdà*, 1998; *Moreno-de las Heras et al*., 2010]. This effect also affects depositional processes as it modulates the availability of eroded materials for deposition in runon areas. In summary, we use the model to address the following questions: (Q1) How do the abiotic factors affecting erosion, and in particular relief, erodibility, and soil diffusion, impact the coevolution of landforms and vegetation? (Q2) What is the effect of the biotic reduction of soil erodibility on the resulting landform-vegetation patterns?, and (Q3) How do vegetation-landform patterns change for a rainfall gradient?

[6] The rest of this paper is organized as follows: section 2 provides a brief description of the coupled dynamic vegetation and landform models used in this work; section 3 describes the numerical experiments to address the research questions described above; and finally, sections 4 and 5 describe the results and some general conclusions.

2. Methods

2.1. Dynamic Vegetation Model

[7] The model for vegetation pattern formation used here is based on previous models [*Rietkerk et al*., 2002; *HilleRisLambers et al*., 2001], which were modified to incorporate seed dispersal by overland flow, and surface water routing that enables its coupling to a landform evolution model [*Saco et al*., 2007]. The model describes the evolution of flow depth (h) as

$$\frac{\partial h}{\partial t} = -\nabla \cdot \boldsymbol{q} + R - \alpha\, h \frac{P + k_2 W_o}{P + k_2}, \tag{1}$$

where q (mm m d^{-1}) represents runoff per unit width, R (mm d^{-1}) is the rainfall rate, P (g m^{-2}) is plant biomass density, α (d^{-1}) represents the maximum rate of infiltration, k_2 (g m^{-2}) is the infiltration saturation constant, W_o (dimensionless) defines the relation between infiltration and biomass density, ∇ is the divergence operator, and vector quantities are indicated by bold italic letters. Equation (1) is solved for steady-state conditions ($\partial h/\partial t = 0$), which is reasonable since the rate of change of runoff is much faster than that at which plant biomass changes occur (days to months). Therefore, a subdaily time step (dt) is used to model vegetation change, and runoff (q) is computed for steady-state conditions (equilibrium values), which occur at much smaller timescales. The direction of the runoff per unit width is computed in the steepest descent and its magnitude, q, is computed using a kinematic wave assumption and Manning's equation as

$$q = \frac{c_n}{n} h^{\frac{5}{3}} S^{\frac{1}{2}}, \tag{2}$$

with n being Manning's roughness coefficient and c_n a unit conversion constant (m $mm^{-2/3}$ d^{-1}). The spatial distribution of overland flow (q) and slope (S) change in response to the evolving topography, resulting from the erosion-deposition processes computed by the landform evolution model. The third term in equation (1) represents the infiltration rate, I, assumed to depend on flow depth h and biomass density P [*HilleRisLambers et al*., 2001; *Rietkerk et al*., 2002]. Bare soil areas have the lowest infiltration rate ($\alpha h W_o$), which increases with biomass density to approach the maximum asymptotic value (αh).

[8] The evolution of soil moisture M is computed as

$$\frac{\partial M}{\partial t} = \alpha\, h \frac{P + k_2 W_o}{P + k_2} - g_{\max} \frac{M}{M + k_1} P - r_m M + D_m \nabla^2 M. \tag{3}$$

Water uptake by plants depends on the availability of soil moisture and is regulated by the maximum specific water uptake $g_{\max}$ (mm g^{-1} m^2 d^{-1}) and the half-saturation constant k_1 (mm). Losses to deep drainage are modeled as a linear function of soil moisture availability with a rate r_m (d^{-1}). Finally, as in previous models [*HilleRisLambers et al*., 2001; *Rietkerk et al*., 2002], redistribution of soil moisture is modeled as a simplified diffusion process with D_m (m^2 d^{-1}) being the soil moisture diffusivity parameter. Changes in plant biomass density P, determined by growth, senescence, and spatial dissemination of vegetation, are modeled as

$$\frac{\partial P}{\partial t} = c\, g_{\max} \frac{M}{M + k_1} P - d\, P + D_p \nabla^2 P - \nabla \cdot \boldsymbol{q_{sd}}, \tag{4}$$

where plant growth is assumed to increase with water uptake, and is determined by the conversion parameter from water uptake to plant growth c (g mm^{-1} m^{-2}), and the maximum asymptotic plant growth rate is given by $cg_{\max}$ (when soil moisture is not limiting). Light availability is assumed not to limit plant growth. Though nutrient limitations can also affect plant growth, the (water) redistribution processes incorporated in the model are assumed to capture spatial redistribution patterns of nutrients as well. d (d^{-1}) is the specific loss coefficient of biomass density due to mortality and D_p (m^2 d^{-1}) is the isotropic plant dispersal coefficient (i.e., due to wind and animal actions). Transport of seed biomass by overland flow is represented by the vector, $\boldsymbol{q_{sd}}$ (g m^{-1} d^{-1}) in the fourth term of equation (4). It has the

direction of overland flow and a magnitude $\boldsymbol{q_{sd}}$ modeled as [*Saco et al.*, 2007]:

$$\begin{aligned} \boldsymbol{q_{sd}} &= c_1 q P \quad \text{for} \quad c_1 q < c_2, \\ \boldsymbol{q_{sd}} &= c_2 P \quad \text{for} \quad c_1 q > c_2, \end{aligned} \tag{5}$$

which assumes both transport-limited conditions for seed redistribution by overland flow, modulated by the parameter c_1 (mm^{-1}), and production-limited conditions determined by the parameter c_2 (m d^{-1}). That is, the maximum seed biomass rate (c_2P) is limited by seed availability, which is assumed to be proportional to the biomass density P.

2.2. Landform Evolution Model

[9] The landform evolution model (SIBERIA) is used to simulate the topographic changes induced by fluvial erosion and diffusive processes (creep and mass movement) [*Willgoose et al.*, 1991; *Willgoose and Riley*, 1998]. Changes in elevations are simulated using mass-transport of sediments over geologic temporal scales. Fluvial sediment transport is modeled using an approach similar to the Einstein-Brown equation, and diffusive processes using a conceptualization of mass movement mechanisms such as creep, rainsplash, and landslide. These processes are averaged in time so that the simulated topography corresponds to the average elevations, giving an indicative average response to the full range of erosive episodes. A detailed mathematical description of this model can be found elsewhere [*Willgoose et al.*, 1991; *Willgoose*, 2005].

[10] The evolution of the elevation at a point, z, is computed using the sediment mass balance:

$$\frac{\partial z}{\partial t} = -(\nabla \cdot \boldsymbol{q_s} + \nabla \cdot \boldsymbol{q_d}) + U, \tag{6}$$

where $\boldsymbol{q_s}$ is the soil transport per unit width ($\text{m}^3\ \text{d}^{-1}\ \text{m}^{-1}$) produced by fluvial processes, $\boldsymbol{q_d}$ is the mass transport of soil material per unit width ($\text{m}^3\ \text{d}^{-1}\ \text{m}^{-1}$) due to diffusive mechanisms, and U (m d^{-1}) is the rate of tectonic uplift.

[11] The magnitude of the sediment transported by runoff, q_s, is computed for transport-limited conditions as

$$\boldsymbol{q_s} = \beta_1\, q^{m_1} S^{n_1}, \tag{7}$$

where q is estimated using equation (2), S is the slope in the steepest downslope direction, β_1 is the rate of sediment transport (similar to the soil erodibility factor in erosion models like CREAMS, USLE), and m_1 and n_1 are the sediment transport coefficients. The parameter β_1 incorporates the dependence (i.e., protective effect) of plant cover on soil erodibility, and assumes a linear decrease in the erosion rate with increasing biomass density [*Boer and Puigdefábregas*, 2005; *Saco et al.*, 2007] as

$$\begin{aligned} \beta_1 &= \beta_b(1 - \beta_v P) \quad \text{for} \quad \beta_v P < 1 - \frac{\beta_{\min}}{\beta_b}, \\ \beta_1 &= \beta_{\min} \qquad\quad \text{for} \quad \beta_v P \geq 1 - \frac{\beta_{\min}}{\beta_b}, \end{aligned} \tag{8}$$

That is, maximum erodibility corresponds to bare soil (β_b) and decreases linearly with increasing biomass density, at a rate β_v ($\text{m}^2\ \text{g}^{-1}$), to a minimum value $\beta_{\min}$.

[12] Sediment transport by diffusive processes is modeled as

$$\boldsymbol{q_d} = DS \tag{9}$$

where D ($\text{m}^2\ \text{d}^{-1}$) is the diffusion coefficient. Mass-wasting processes like debris flows and landslides are not considered because they are not relevant for the range of slopes analyzed in this study.

2.3. Coupled Model

[13] The landform (SIBERIA) and vegetation evolution models are coupled through the hydrologic (runoff-runon), ecologic (biomass density), and geomorphic (slope and elevation) variables, which are shared between them. Even though the models have a common computational grid, the processes simulated in each of them are executed using different time steps because they operate at different temporal scales. SIBERIA's time step is selected for an appropriate representation of erosion rates (days to years), whereas the vegetation model operates at shorter time steps (subdaily) to capture infiltration and water-redistribution processes. A tighter coupling between the models has not been implemented to preserve computational performance and speed. The information is transferred between the models in several steps. First, the vegetation model computes the spatial distribution of overland flow and vegetation density (runoff-runon fluxes that depend on vegetation through the effects of water uptake and enhanced infiltration rates under plants). Then, those values for biomass and surface flow are supplied to the landform evolution model to compute sediment transport. During this step, biomass information is used to set the erodibility values, and water fluxes are used to compute the spatial distribution of erosional and depositional volumes and to update topography. Finally, the new elevations are used to determine updated slopes and flow directions that are input into the next step of the vegetation model.

3. Design of Numerical Experiments

[14] All simulations were designed to analyze coevolution of vegetation and landforms in a 200 m × 200 m hillslope, using a grid size of 2 m. No-flow boundary conditions were used for both the lateral and upstream borders, and a free-flow boundary condition was used in the downstream border. A no-flow boundary condition was used at the hilltop to capture realistic landscape boundaries (as opposed to the periodic boundary condition normally used in models of vegetation pattern formation).The initial landforms used for the simulations consist of hillslopes with varying initial slopes of 1–2% (typically found in the banded vegetation landscapes of Australia [*Tongway and Ludwig*, 2001; *Moreno-de las Heras et al.*, 2011a]), and with small perturbations added to the initial elevations (i.e., values drawn from a uniform random distribution in the interval [−0.1, 0.1]). The initial vegetation consisted of biomass peaks of 50 g m^{-2} randomly distributed in 1% of the grid elements on an otherwise bare hillslope. Other initial conditions were also used (i.e., random perturbations of a continuous biomass cover) to check that final results were not affected by the initial conditions.

[15] Parameters for vegetation dynamics used in this analysis were selected following the ones presented by *Rietkerk et al*. [2002], *HilleRisLambers et al*. [2001], and *Saco et al*. [2007]. Though field studies report the existence of both migrating and stationary patterns [*Valentin et al*., 1999; *Tongway and Ludwig*, 2001], by selecting appropriate values of c_2 [*Saco et al*., 2007] we simulate landscapes with no upslope migration of vegetation as those found in Australia [*Deblauwe et al*., 2012; *Dunkerley and Brown*, 2002; *Dunkerley*, 2002]. Parameters for the landform evolution model utilized for all simulations were selected from the values recommended on previous studies [*Willgoose*, 2005].

[16] The initial conditions, boundary values, and general set of model parameters described above were used in all simulations and are displayed in the caption of Figure 2. In section 3.2, we describe specific details of the set of simulations used to address the individual research questions described in the introduction.

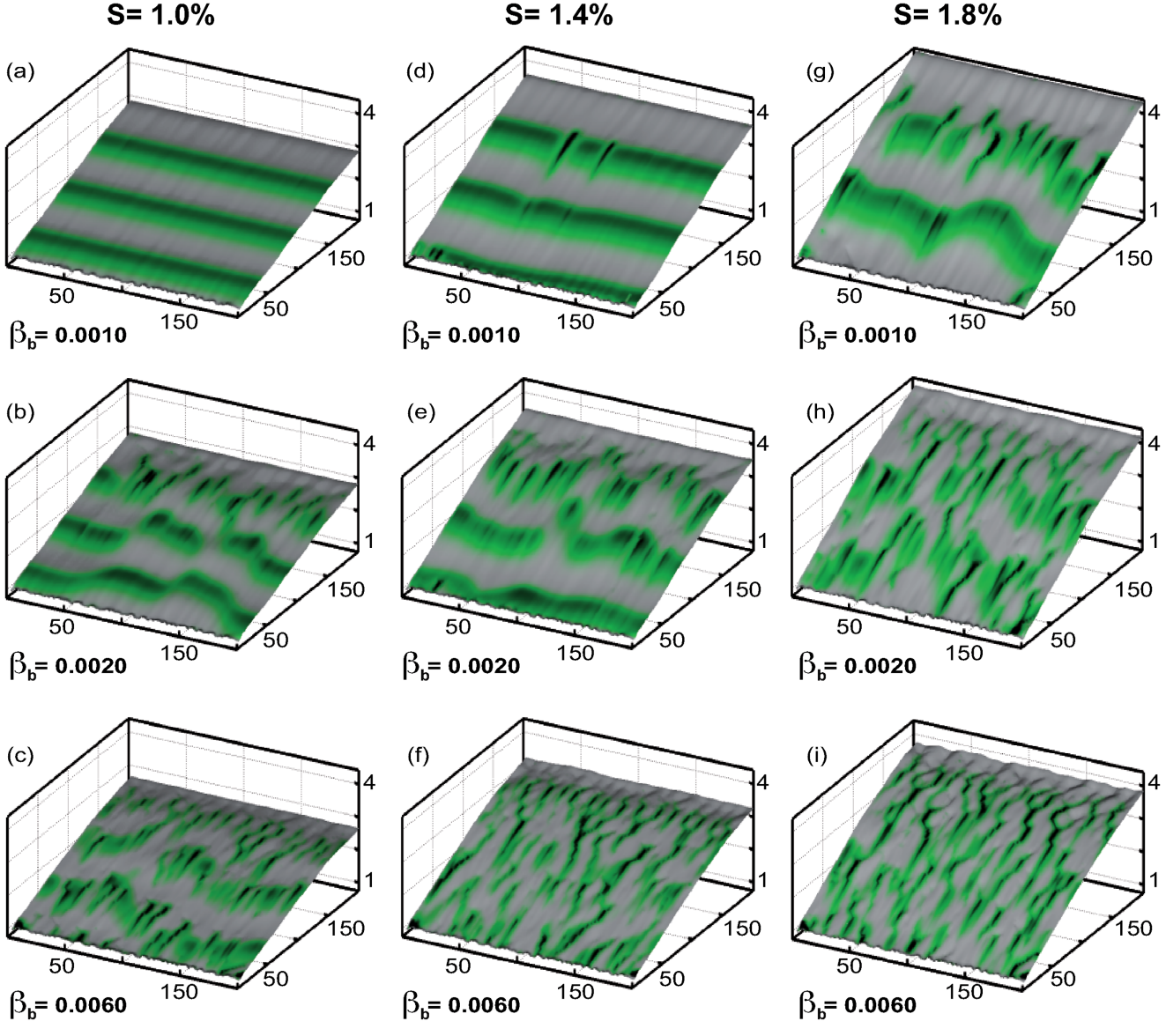

Figure 2. Simulation results for both landforms and vegetation patterns (biomass density is shown in green) after 1000 years. Different columns correspond to simulations with varying initial slopes (S = 1%, 1.4%, and 1.8%), and rows correspond to simulations with different erodibility values (β_b = 0.001, 0.002, and 0.006). Parameters used in simulations for the vegetation model are: R= 350 mm yr^{-1}, n = 0.05, k_2 = 12 g m^{-2}, W_o = 0.2, D_m = 0.27 m^2 d^{-1}, g_{max} = 0.05 mm g^{-1} m^2 d^{-1}, k_1 = 5 mm, r_m = 0.19 d^{-1}, c = 10 g mm^{-1} m^{-2}, d = 0.24 d^{-1}, D_p = 0.3 m^2 d^{-1}, c_1 = 2.25 mm^{-1}, c_2 =0.14 m d^{-1}. Parameters for the landform model are D = 0.05 m^2 s^{-1}, U = 0, m_1 = 1.8, n_1 = 1.1, β_v = 0.0028 m^2 g^{-1}, β_{min} = 0, dt = 0.5 day. Note: shades of green are used to represent biomass densities (P), with darker shades denoting higher values of P.

3.2. Simulations Designed to Address Research Questions

3.2.1. Q1: How Do the Abiotic Factors Affecting Erosion, Specifically Relief, Erodibility, and Soil Diffusion, Impact the Coevolution of Vegetation-Landform Patterns?

[17] We investigate the mechanisms and feedbacks between erosion, water redistribution, and vegetation growth that give rise to different patterns (banded vegetation perpendicular to flow directions, stripes along drainage lines, or mixed patterns). Specifically, we analyze the emergence of these patterns in relation to key parameters associated to both water and sediment partition and redistribution, which affect vegetation and landforms processes and feedbacks. As mentioned in the introduction, slope is a key parameter that determines the partition of runoff and infiltration. It also plays an important role in sediment redistribution [*Wilcox et al*., 2003], though its influence is modulated by soil erodibility and diffusion processes [*Willgoose et al*., 1991; *Willgoose and Riley*, 1998]. Consequently, simulations were designed to investigate the coevolution of vegetation and landforms for different initial slopes, and for a range of bare soil erodibility and soil diffusion values (see Table 1). The range of parameter values was broad enough and suitable to study the formation of different vegetation-landform patterns and transitions between the banded and striped patterns observed in many semiarid environments.

3.2.2. Q2: What Is the Direct Effect of the Biotic Reduction of Soil Erodibility on the Resulting Landform-Vegetation Patterns?

[18] Vegetation changes soil redistribution by modifying both water redistribution and soil erodibility. The effect of water redistribution induced by the emergence of areas with lower (higher) infiltration that constitute sources (sinks) of runoff and affect fluvial erosion patterns [*Valentin et al*., 1999; *Wilcox et al*., 2003] is captured in all the simulations (i.e., those addressing all research questions). In Q2, we focus on understanding how different degrees of erodibility reduction by plants, which affect feedbacks between vegetation, fluvial erosion, and landforms, alter the resulting vegetation patterns.

[19] The effect of vegetation on erodibility is isolated by running the model with different values of β_v (see equation (8)). We performed 1000 years-long simulations for an initial slope of 1.4% (an intermediate slope), and the range of values of soil erodibility and diffusion (β_b, D) and vegetation control on erosion (β_v) displayed in Table 1. All other parameter values were the same than for Q1.

3.2.3. Q3: What Is the Effect of Increasing Rainfall Rates on the Vegetation-Landform Patterns?

[20] To address this question, we run 1000 years-long simulations for a range of annual rainfall rates (shown in Table 1). This range of rainfall intensities (typical of arid to semiarid areas) was selected to produce all possible vegetation conditions from complete bare-soil hillslopes to a complete vegetation cover.

Table 1. Parameters Used in Simulations to Address Research Questions (Q1, Q2, and Q3)

	S (%)	β_b ($m^2\ g^{-1}$)	D ($m^2\ s^{-1}$)	β_v ($m^2\ g^{-1}$)	R ($mm\ yr^{-1}$)
Q1	1–2	0.0001–0.006	0.01–0.1	0.0028	350
Q2	1.4	0.0001–0.006	0.01–0.1	0.0028–0.05	350
Q3	1.4	0.0001–0.006	0.01–0.1	0.0028	200–600

4. Results and Discussion

4.1. Q1: Impact of Relief, Erodibility, and Soil Diffusion on the Coevolution of Vegetation-Landform Patterns: Self-Organization Into Landforms With Banded, Mixed, and Striped Vegetation Patterns

[21] Results from 540 simulations for a period of 1000 years were analyzed for the range of initial slopes, bare soil erodibility, and soil diffusion parameters shown in Table 1. Though these simulations produced a broad range of vegetation-landform patterns, the results can be broadly classified by visual inspection into three main distinct categories: landscapes that evolve into banded vegetation patterns in landforms displaying smooth topography with no rills (pattern 1), landscapes showing mixed patterns, that is, where both banded vegetation and striped patterns coexist in the hillslope (pattern 2), and landscapes showing the formation of vegetation stripes along distinct rills that are present throughout the hillslope (pattern 3).

[22] Figure 2 illustrates the typical patterns obtained from the coevolution of landforms and vegetation for 1000 years-long model runs. All landscapes in this figure were obtained from simulations using a soil diffusion parameter $D = 0.05\ m^2\ s^{-1}$. Different columns correspond to landforms with varying initial slopes (S = 1%, 1.4%, and 1.8%), and different rows correspond to simulations with different bare soil erodibility values (β_b = 0.001, 0.002, and 0.006). These plots show examples of the three patterns used in the classification, that is, pattern 1: banded (Figures 2a and 2d), pattern 2: mixed (Figures 2b, 2e, and 2g), and pattern 3: stripes along drainage lines with higher-flow concentration (Figures 2c, 2h, 2f, and 2i).

[23] As shown in Figure 2, for hillslopes with lower fluvial erosion (low erodibility and/or lower slope gradients), the system evolves into banded vegetation with varying degree of undulated or stepped microtopography (Figures 2a and 2d). As explained in more detail in the next section, the dynamic behavior of this stepped microtopography is consistent with field observations [*Dunkerley and Brown*, 1995, 1999]. Higher values of fluvial erosion and/or higher slopes give rise to flow concentration and vegetation growth along depressions and drainage lines. In this case, the hillslope tends to develop microtopographic features consistent with flow concentration (Figures 2c, 2h, and 2f) and surface water connectivity increases through the development of rills connecting larger portions of the hillslope. For the higher slopes and soil erodibilities, rills connecting the entire hillslope tend to develop (Figure 2i). Interestingly, these rills are not static; they change position with time and preserve a state of dynamic equilibrium induced by vegetation effects on sediment deposition. On the one hand, rills concentrate flow and therefore with time they are colonized by vegetation; on the other hand, once a high biomass cover is achieved, they tend to disappear over time because of the lower erodibility induced by vegetation cover and the deposition of sediments induced by runon mechanisms. The bare areas that are subject to erosion develop new rills that are eventually colonized by vegetation.

This process continues and maintains a state of temporal dynamic equilibrium. In the mixed hillslopes (Figures 2b, 2e, and 2g) both bands and stripes are present, and a mixture of microtopographic features, like rills in the upper portion and undulations in the lower portion of the simulated hillslopes, coexist.

[24] Using the reference patterns described above and illustrated in Figure 2, and for each initial slope, the values of the soil parameters β_b and D for which a transition occurs from banded to mixed patterns (T1), and from mixed to striped patterns (T2) were identified using the results from the 540 simulations. A phase diagram displaying the areas corresponding to banded, mixed and striped patterns as a function of S and β_b, for simulations with $D = 0.05$ m^2 s^{-1} is presented in Figure 3a. The lines in Figure 3 indicate the transitions, and the dots show the sets of parameters used to obtain the simulated landscapes displayed in Figure 2. The dashed line in this diagram corresponds to T1 transitions, that is, parameters below this line (S and β_b) give rise to banded pattern formation and topographic profiles with parallel drainage lines and no flow accumulation (similar to those of Figures 2a and 2d). The area above this dashed line corresponds to conditions of S and β_b that result in mixed patterns (bands and stripes, as shown in Figures 2b, 2e, and 2g). The continuous line shows the transition from the mixed to striped patterns. Above this line, and due to the prevalence of fluvial erosion, landscapes develop rills and a pattern of vegetation stripes along these rills due to the presence of higher water availability.

[25] Figures 3b and 3c display phase diagrams summarizing transitions (T1 and T2) for different values of the soil diffusion parameter (D). The curves shown in Figures 3a–3c were obtained from a bicubic spline interpolation on the values identified for the transitions (T1 and T2). From this interpolation, we obtained two smooth surfaces (D as a function of S, β_b) whose projections (i.e., curves for different values of D) are shown in Figure 3.

[26] As expected, banded patterns are predominantly found for the lower soil erodibility values, but values of soil diffusion are also important in determining pattern formation. This is due to the fact that it is the interplay between diffusive and fluvial erosion processes interacting with vegetation (which affects runoff partition) that determines the evolutionary trajectory of the landform-vegetation pattern. For example, results for any initial slope (vertical lines in Figure 3b) show that, as D increases, banded patterns can be found for semiarid regions with higher soil erodibility. Alternatively, for the same soil erodibility (horizontal line in Figure 3), bands can be found in hillslopes with higher relief if soil diffusion processes are high. These results can therefore explain observations by *Valentin et al.* [1999], who reported that banded patterns can be found in a very wide range of slopes, from gentle slopes (where they are more commonly observed) to steeper slopes like those of southeastern Spain [*Sánchez*

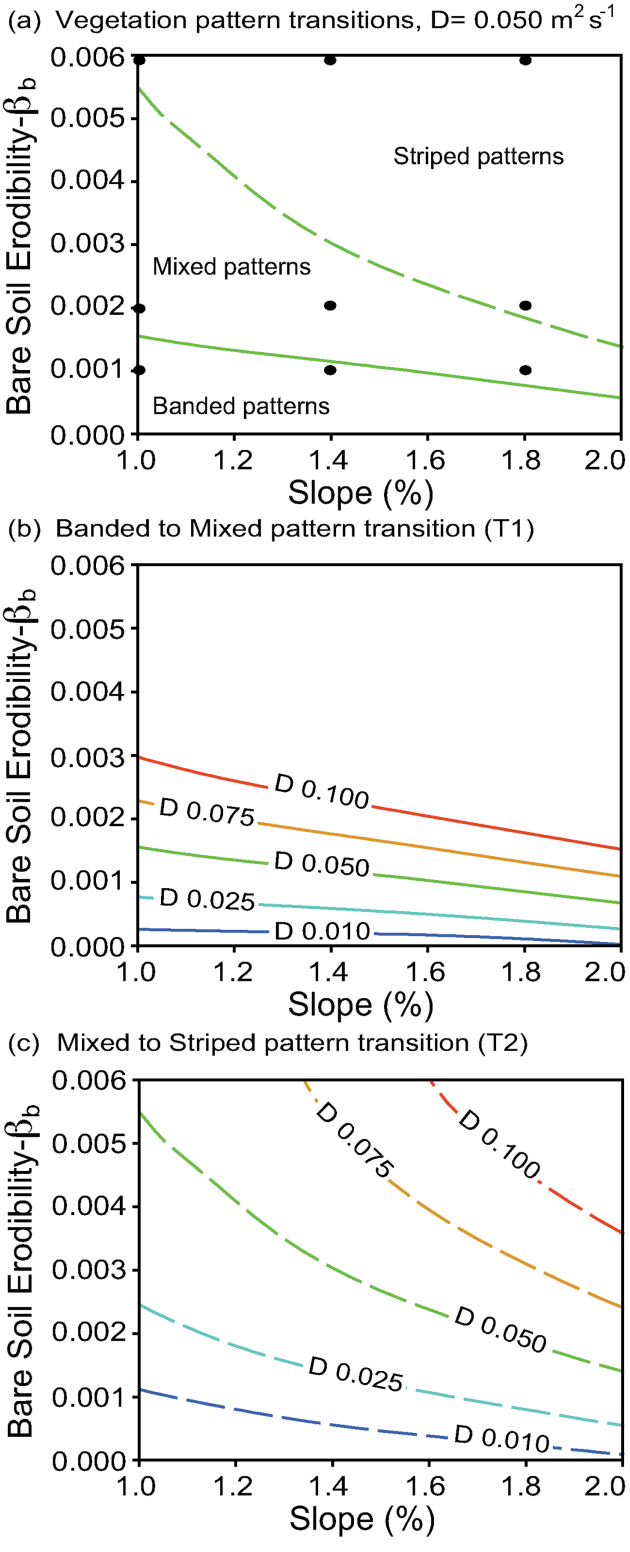

Figure 3. Phase diagrams displaying areas for simulation parameters (S, bare soil erodibility β_b) leading to banded, mixed, and striped patterns. (a) For $D = 0.05$ m^2 s^{-1}, the lines in Figure 3 show transitions between banded patterns (area below the continuous line), mixed patterns (area between continuous and dashed lines), and patterns with stripes along rills (area above dashed line). The dots indicate parameter values used to obtain landscapes displayed in Figure 2. (b) Transitions between banded and mixed patterns (T1) for varying values of D. (c) Transitions between mixed and striped patterns (T2) for varying values of D. All other parameters used in the simulations to obtain this figures are listed in Figure 2.

and Puigdefábregas, 1994; *Puigdefábregas and Sánchez*, 1996; *Bergkamp et al.*, 1999].

[27] Figure 4 shows topographic transects along the middle sections of the landform profiles for 1000 years-long simulations with an initial slope $S = 1\%$ and soil diffusion $D = 0.075$ m^2 s^{-1}. These transects allow for a better comparison of how local (micro) and hillslope-scale topography changes with increasing soil erodibility. For the lower values of erodibility ($\beta_b = 0.0001$ to $\beta_b = 0.0020$) displayed in the bottom four profiles, the vegetation-landform pattern self-organizes into a banded system. As seen in these profiles, feedbacks between water redistribution and vegetation give rise to the emergence of three distinct vegetation bands (green dashed lines) and to an undulated or mild stepped microtography that coevolved with those bands. Note that in this case runoff occurs as sheet flow with parallel flowlines (perpendicular to the vegetation bands) and no flow concentration. The undulated or stepped microtopography is more pronounced for the higher erodibility ($\beta_b = 0.0020$). This could be expected since the higher erodibility produces more sediment redistribution in the landscape with higher erosion in the bare areas of the vegetation patterns (note that, for this range of erodibility values, the resulting vegetation banded patterns are very similar). The general decrease in final slopes with increasing erodibility is also clear in these profiles. For higher erodibility values ($\beta_b > 0.0020$), fluvial erosion generates rills with concentration of flow (top two profiles). The vegetation pattern then changes to a striped pattern, and therefore the biomass density (green dashed line) in these profiles represents only local conditions. As seen in Figure 4, the stepped microtopography disappears for the higher erodibility, and the microtopography is generated by the rills (these can only be appreciated in three-dimensional profiles as those shown in Figure 2).

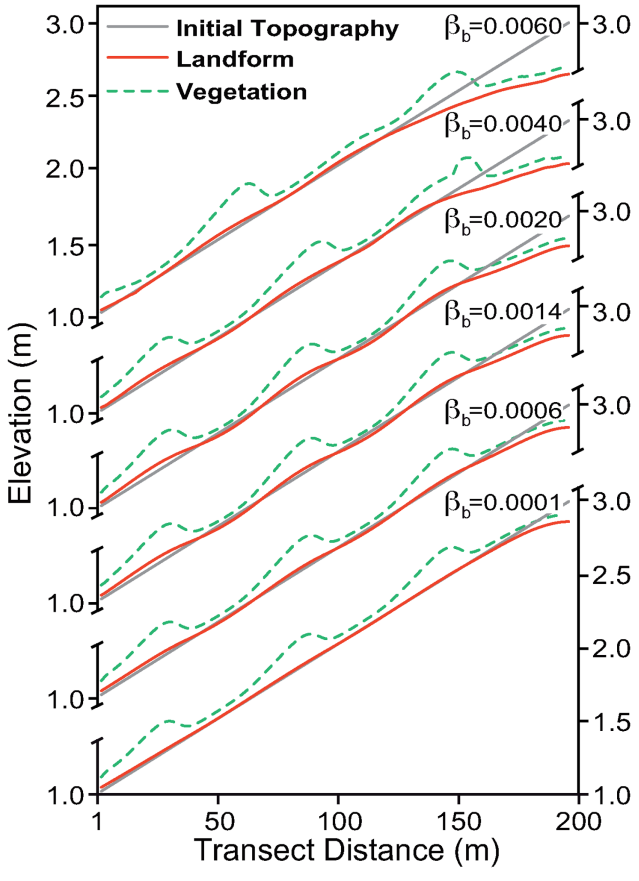

Figure 4. Topographic transects for 1000 years-long simulated landforms, with initial slopes of 1% (depicted by solid gray lines), $D = 0.075$ m^2 s^{-1}, and varying soil erodibities (displayed in the figure legend). Note: to allow for easy visual comparisons, the y axis (elevations in m) only represents the vertical scale of elevations in meter. Changes in the topographic profile after 1000 years can be measured relative to the initial topography shown by the gray lines (it is the same for all simulations).

4.2. Q2: Effect of the Biotic Reduction of Soil Erodibility on Landform-Vegetation Patterns

[28] As explained before, the effect of reduction of soil erodibility by vegetation was analyzed by running simulations with varying values of the parameter β_v, which represents a linear reduction in the rate of erodibility with increasing biomass density (equation (8)). Figure 5 allows for the comparison of simulation results after 1000 years, for values $\beta_v = 0.0028$ and 0.05 m^2 g^{-1}. This range of values can be interpreted in terms of erodibility reduction in areas of high biomass as follows: for the maximum values of biomass obtained within the patterns ($P = 50$ g m^{-2}), $\beta_v = 0.0028$ m^2 g^{-1} induces reductions in erodibility of up to 15% ($\beta_1 = 0.85\ \beta_b$ in equation (8)), while $\beta_v = 0.05$ m^2 g^{-1} drastically reduces erodibility to its minimum value (in this case, $\beta_1 = \beta_{min} = 0$, so the reduction is 100% in areas of high biomass).

[29] Figures 5a and 5b show results for simulations using $D = 0.075$ m^2 s^{-1}, $\beta_b = 0.001$, and an initial slope $S = 1.4\%$. These values indicate prevailing diffusive processes leading to banded profiles (see phase diagram in Figure 3b, obtained for $\beta_v = 0.0028$ m^2 g^{-1}). Figure 5b shows that the banded hillslope profile obtained for $\beta_v = 0.05$ m^2 g^{-1} displays a stepped microtopography that is remarkably more pronounced than the slightly undulated microtopography obtained for the lower $\beta_v = 0.0028$ m^2 g^{-1} (Figure 5a). This is a reasonable consequence of the drastic reduction in erodibility localized in vegetated areas for the high values of β_b. Vegetation patterns for both simulations display an almost identical biomass distribution because the small variations in slope induced by the stepped microtopography have a negligible influence in the vegetation pattern. As seen in Figure 5, a large portion of the vegetated bands are located in the regions of higher slope between bare and vegetated areas. The appearance of this type of stepped hillslope profile has been observed in numerous field sites with banded vegetation [*Slatyer*, 1961; *Mabbutt and Fanning*, 1987; *Berg and Dunkerley*, 2004; *Tongway and Ludwig*, 1990; *Puigdefábregas and Sánchez*, 1996]. As observed by *Dunkerley and Brown* [1999] in banded acacia shrubland and chenopod shrubland communities in Australia, each step is composed of an upper grove and lower intergrove, has a concave-upward shape, and constitutes a source-sink unit. This sink-source functioning produces erosion in the intergrove areas that increases with distance from the upper grove boundary. The highest runoff at the boundary of the

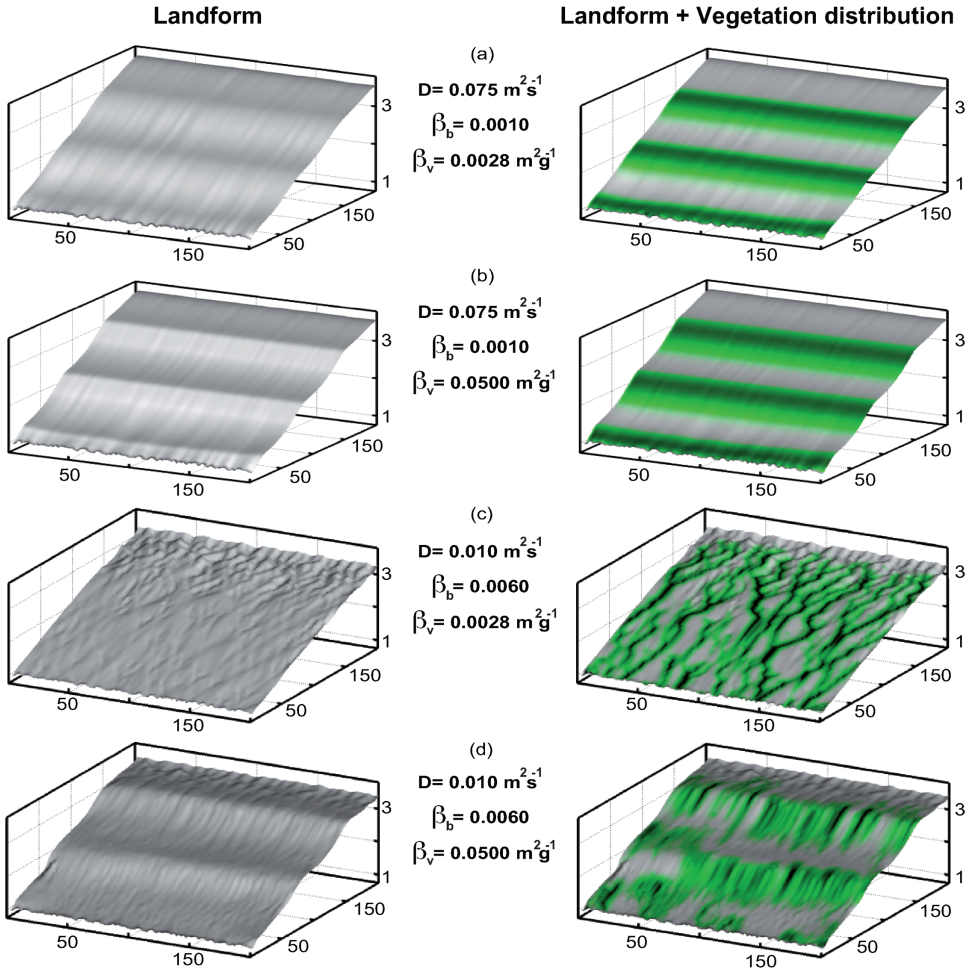

Figure 5. Simulation results showing (left) landforms and (right) vegetation patterns for an initial slope of 1.4%, after 1000 years. (a and b) Changes induced by varying the effect of biomass on erodibility (β_v = 0.0028 and 0.05 m^2 g^{-1}) for a landscapes with prevailing soil diffusion processes (D = 0.075 m^2 s^{-1}, β_b = 0.001) that leads to banded pattern formation. (c and d) Changes for a landscape with prevailing fluvial erosion processes (D = 0.01 m^2 s^{-1}, β_b = 0.006) that lead to striped pattern formation.

grove induces high infiltration and depositional rates, giving rise to the concave-upward elements.

[30] Figures 5c and 5d enable the comparison of simulation results for the same initial S = 1.4%, and parameter values D = 0.01 m^2 s^{-1} and β_b = 0.006. As seen in the phase diagram of Figure 3c, these parameters are well above the transition T2 (dark blue dashed line), which means that the pattern for β_v = 0.0028 m^2 g^{-1} displays clear vegetation stripes along drainage rills. The corresponding pattern, shown in Figure 5c, shows the small rills spanning the entire hillslope, which therefore induces surface water connectivity along the complete profile (i.e., top to bottom) and stripes of vegetation along those rills. In the simulations with higher erodibility reduction by vegetation (β_v = 0.05 m^2 g^{-1}, Figure 5d) there are still vegetation stripes in drainage lines with high flow concentration, but rills do not span the entire hillslope. The effect of the coevolving vegetation generates in this case a feedback effect that inhibits the formation of long rills. The final pattern displays some of the regularity of banded patterns (and limited surface water connectivity), which leads to the emergence of a clearly stepped microtopography. However, it still displays some short rills induced by the higher fluvial erosion in areas of lower vegetation cover.

4.3. Q3: Effect of Varying Annual Rainfall Rates on Vegetation-Landform Patterns

[31] Figure 6 shows the effect of increasing rainfall in the resulting simulated landform-vegetation patterns. Simulations shown correspond to an initial slope S = 1.4%, D = 0.06 m^2 s^{-1}, β_v = 0.0028 m^2 g^{-1}, and β_b = 0.0007 (banded patterns shown in the left column) or β_b = 0.006 (striped patterns shown on right column). For lower values of yearly rainfall (R = 200 mm yr^{-1}) biomass disappears (i.e., P = 0), while for higher values (R > 550 mm yr^{-1}), bare areas disappear and the biomass covers the entire hillslope.

[32] As seen in the left column of Figure 6, for banded hillslopes with low fluvial erosion (β_b = 0.0007), as rainfall increases the number of bands increases and the interband length decreases. The landforms shown in Figure 6, for the banded hillslopes, show the effect of higher denudation rates for higher rainfall values, with an overall decrease in

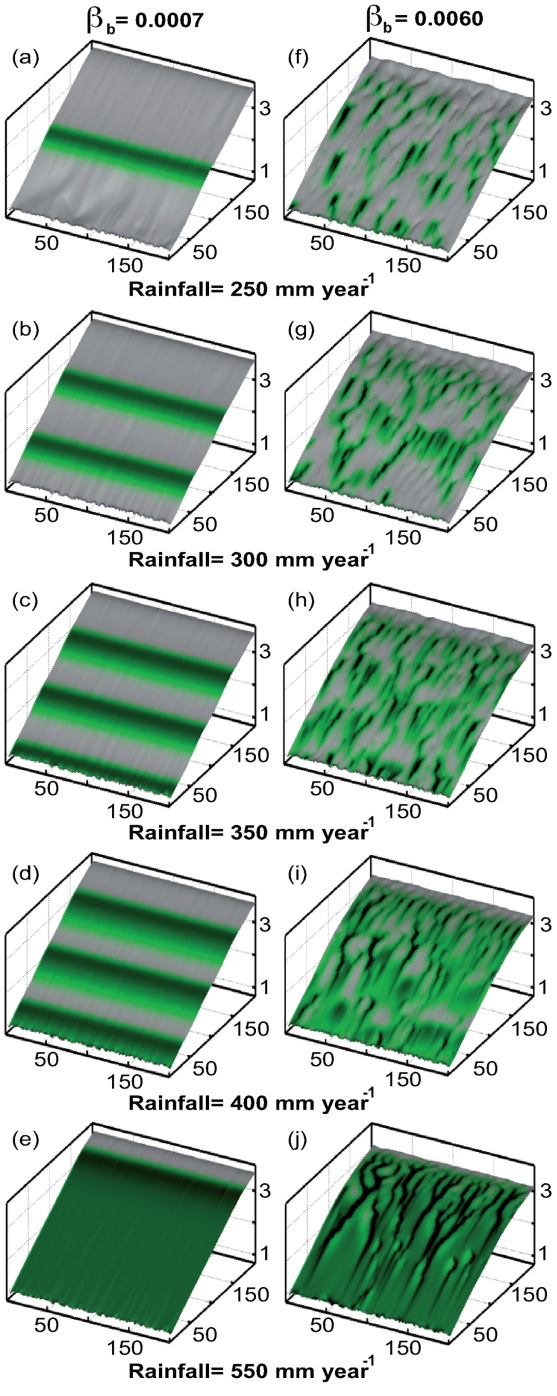

Figure 6. Landforms (shades of gray) and vegetation patterns (shades of green) obtained for 1000 years-long simulations for and initial slope $S = 1.4\%$ and $D = 0.06$ m^2 s^{-1}. Rows show results for increasing of rainfall values (R is shown below figures) and erodibility ($\beta_b = 0.0007$ m^2 g^{-1} for figures in the left column, and $\beta_b = 0.006$ m^2 g^{-1} for figures in the right column).

elevations (and slope) for higher precipitation (though the change in elevations is small and therefore not too obvious in these plots). These landforms, for all R values, are characterized by a smooth topographic profile with no flow concentration and by the presence of undulated microtopography with mild steps coevolving with the emerging vegetation bands (as discussed in Q2, for low β_b and $\beta_v = 0.0028$ m^2 g^{-1} the stepped microtopography is mild). In this case (low erodibilty), changes in vegetation pattern organization with increasing rainfall are in general agreement with previous results for fixed topographies [*von Hardenberg et al*., 2001; *Rietkerk et al*., 2002]. However, we should note these previous models, due to the lack of landform-vegetation interactions, cannot reproduce the patterns on the right column of Figure 6, which are obtained from the same planar initial hillslopes.

[33] For the higher erodibility ($\beta_b = 0.006$) case, fluvial erosion prevails over soil diffusion processes and landforms develop small rills even for low rainfall values (i.e., $R = 250$ mm yr^{-1}). Changes in landforms with increasing R reflect an increase in rilling due to the higher fluvial erosion, and an increase in biomass density along rills that tends to a complete cover as R continues to increase (i.e., for $R = 550$ mm yr^{-1}). Interestingly, the vegetation cover is not uniform (as predicted by models of vegetation pattern formation that do not consider landform feedbacks), and maintains a higher density on areas of high water concentration (higher biomass density is represented by darker shades of green).

5. Summary and Conclusions

[34] During the last decade, significant efforts have been devoted to understanding feedbacks and nonlinear interactions between water redistribution and vegetation patterns in semiarid areas from a purely ecohydrologic perspective. Modeling studies on the coevolution of landforms and vegetation have been very scarce, and just a couple of those did account for the effect of patchy vegetation cover. We showed here that it is necessary to consider the coevolving landform-vegetation system to begin to understand the richness of patterns found in semiarid areas.

[35] Some general results from our work on pattern formation accounting for landform-vegetation coevolution follow: Results from our simulations are consistent with field's observations showing that banded patterns tend to appear on gentle slopes, where there is no overland flow concentration [*Valentin et al*., 1999]. However, our results also suggest that the appearance of banded patterns in areas with higher relief, though unusual, is still possible if diffusion processes are dominant and, in particular, if the effect of vegetation on soil protection is significant. Moreover, a decrease in soil erodibility by vegetation cover, for example by plant species that have a substantial soil protective effect, tends to accentuate stepped microtopographic features generated by sediment redistribution in banded patterns. These results are consistent with the existence of banded vegetation patterns in higher relief areas of southeastern Spain, which are associated with the presence of a pronounced stepped microtopography [*Sánchez and Puigdefábregas*, 1994; *Puigdefábregas and Sánchez*, 1996; *Bergkamp et al*., 1999], and according to our simulations suggest a dominant role of vegetation on erodibility reduction.

[36] Though banded patterns in high relief areas are possible, our results show that it is more likely to find concentrated flow leading to vegetation stripes, that is, plant growth along drainage lines (an extremely common pattern in semiarid areas). Moreover, we showed that small variations in

slope and/or abiotic (soil erodibility or diffusivity) and biotic (plant species with varying protective effects on erodibility) factors can give rise to changes from banded to striped patterns.

[37] We found that for banded landscapes, as rainfall increases the vegetation pattern changes, with an increase in the number of bands and a decrease in interband length, which is in agreement with previous results for fixed topographies [*von Hardenberg et al*., 2001; *Rietkerk et al*., 2002]. For high rainfall values, vegetation tends to a continuous cover with uniform biomass density. Interestingly, for the case of landscapes dominated by fluvial erosion, as rainfall increases, vegetation also tends to completely cover all the hillslope, but biomass density is not uniformly distributed. In this case, the landform-vegetation pattern coevolves, giving rise to the formation of rills and vegetation stripes that increase in number (density) and extension with increasing rainfall. For higher rainfall, vegetation tends to cover the complete hillslope, but higher biomass density is still located in the rills. Note that these results were obtained for gentle slopes, in which it is possible to assume that rill flow and erosion do not affect plant survival.

[38] In summary, we showed that self-organized vegetation patterns strongly depend on feedbacks with coevolving landforms, and that patterns change depending on the prevailing erosion rates and mechanisms (prescribed by slopes and dominance or either fluvial or diffusive processes), which in turn are affected by biotic factors related to vegetation cover protection. Therefore, our results reinforce the importance of analyzing the coevolution of landforms and vegetation in order to improve our understanding of the patterns and structures found in nature, and particularly in semiarid regions. Moreover, we showed that the ecohydrologic processes leading to banded pattern formation, represented in the models currently used in the literature, if coupled with landform processes, can also lead to completely different patterns (stripes of vegetation along drainage lines) that are equally commonly found in nature.

[39] The model described in this paper incorporates a description of mechanistic process in response to constant, long-term mean, environmental parameters and rainfall rates. The analysis is designed to capture trends at the longer timescales needed for modeling landform evolution processes and enable the identification of equilibrium states in isolation from transient processes. Changes in mean rainfall rates have been investigated and, though transient behaviors are observed, simulations show transitions between the equilibrium patterns. That is, provided rainfall intensities are sustained for long-enough periods, the system approaches a new equilibrium state corresponding to the new rainfall intensity (shown in Figure 6).

[40] Changes in rainfall variability induced by climate change (e.g., rainfall rate distribution with more pronounced extreme events) need to be investigated in future research, as they could produce shifts leading to vegetation and soil losses, particularly in steeper slopes prone to erosion. Considerations on how atmospheric CO_2 could affect biomass production, which are extremely important to address impacts due to climate change, have not been considered here, and also need to be considered in future work.

[41] Sustainable management of drylands requires the development of action plans driven by science-based understanding of arid and semiarid ecosystems [*Tongway and Ludwig*, 2001; *Turnbull et al*., 2008]. In this respect, coupled vegetation-landform modeling supply essential information to bridge the gap between land-management policy and scientific knowledge. They provide integrative tools for predicting ecosystem response and facilitate the design of restoration/mitigation strategies that ensure long-term stability under current climate and land-use changes.

[42] **Acknowledgments.** This work was partially supported by a grant from the Australian Research Council (DP0774184). The authors thank the Editor Graham Sander, the Associate Editor Michael L. Roderick, and two anonymous reviewers for providing helpful comments and suggestions to improve the manuscript.

References

Baas, A. C. W., and J. M. Nield (2007), Modelling vegetated dune landscapes, *Geophys. Res. Lett.*, *34*, L06405, doi:10.1029/2006GL029152.

Belnap, J., J. R. Welter, N. B. Grimm, N. Barger, and J. A. Ludwig (2005), Linkages between microbial and hydrologic processes in arid and semiarid watersheds, *Ecology*, *86*(2), 298–307.

Berg, S. S., and D. L. Dunkerley (2004), Patterned Mulga near Alice Springs, central Australia, and the potential threat of firewood collection on this vegetation community, *J. Arid Environ.*, *59*, 313–350.

Bergkamp, G., A. Cerda, and A. C. Imeson (1999), Magnitude-frequency analysis of water redistribution along a climate gradient in Spain, *Catena*, *37*, 129–146.

Boer, M., and J. Puigdefábregas (2005), Effects of spatially structured vegetation patterns on hillslope erosion in a semiarid Mediterranean environment: A simulation study, Effects of vegetation patterns on erosion, *Earth Surf. Processes Landforms*, *30*, 149–167.

Borgogno, F., P. D'Odorico, F. Laio, and L. Ridolfi (2009), Mathematical models of vegetation pattern formation in ecohydrology, *Rev. Geophys.*, *47*, 1–36, doi:10.1029/2007RG000256.

Caylor, K. K., T. M. Scanlon, and I. Rodríguez-Iturbe (2009), Ecohydrological optimization of pattern and processes in water-limited ecosystems: A trade-off-based hypothesis, *Water Resour. Res.*, *45*, W08407, doi:10.1029/2008WR007230.

Cerdà, A. (1998), Soil aggregate stability under different Mediterranean vegetation types, *Catena*, *32*, 73–86.

Collins, D. B. G., and R. L. Bras (2010), Climatic and ecological controls of equilibrium drainage density, relief, and channel concavity in drylands, *Water Resour. Res.*, *46*, W04508, doi:10.1029/2009WR008615.

Corenblit, D., and J. Steiger (2009), Vegetation as a major conductor of geomorphic changes on the Earth surface: Toward evolutionary geomorphology, *Earth Surf. Processes Landforms*, *34*, 891–896, doi:10.1002/esp.1788.

Deblauwe, V., P. Couteron, J. Bogaert, and N. Barbier (2012), Determinants and dynamics of banded vegetation pattern migration in arid climates, *Ecol. Monogr.*, *82*, 3–21, doi:10.1890/11-0362.1.

Dunkerley, D. L. (2002), Infiltration rates and soil moisture in a groved Mulga community near Alice Springs, arid central Australia: Evidence for complex internal rainwater redistribution in a runoff runon landscape, *J. Arid Environ.*, *51*, 199–219.

Dunkerley, D. L., and K. J. Brown (1995), Runoff and runon areas in a patterned chenopod shrubland, arid western New South Wales, Australia: Characteristics and origin, *J. Arid Environ.*, *30*, 41–55.

Dunkerley, D. L., and K. J. Brown (1999), Banded vegetation near Broken Hill, Australia: Significance of surface roughness and soil physical properties, *Catena*, *37*(1–2), 75–88.

Dunkerley, D. L., and K. J. Brown (2002), Oblique vegetation banding in the Australian arid zone: Implications for theories of pattern evolution and maintenance, *J. Arid Environ.*, *51*, 163–181.

Franz, T. E., K. K. Caylor, J. M. Nordbotten, I. Rodríguez-Iturbe, and M. A. Celia (2010), An ecohydrological approach to predicting regional woody species distribution patterns in dryland ecosystems, *Adv. Water Resour.*, *33*(2), 215–230, doi:10.1016/j.advwatres.2009.12.003.

HilleRisLambers, R., M. Rietkerk, F. van den Bosch, H. H. T. Prins, and H. de Kroon (2001), Vegetation pattern formation in semi-arid grazing systems, *Ecology*, *82*(1), 50–61.

Kéfi, S., M. Rietkerk, C. L. Alados, Y. Pueyo, V. P. Papanastasis, A. ElAich, and P. C. de Ruiter (2007), Spatial vegetation patterns and imminent desertification in Mediterranean arid ecosystems, *Nature*, *449*, 213–217, doi:10.1038/nature06111.

Ludwig, J. A., B. P. Wilcox, D. D. Breshears, D. J. Tongway, and A. C. Imeson (2005), Vegetation patches and runoff-erosion as interacting ecohydrological processes in semiarid landscapes, *Ecology*, *86*(2), 288–297.

Mabbutt, J. A., and P. C. Fanning (1987), Vegetation banding in arid Western Australia, *J. Arid Environ.*, *12*, 41–59.

Mayor, A. G., S. Bautista, E. E. Small, M. Dixon, and J. Bellot (2008), Measurement of the connectivity of runoff source areas as determined by vegetation pattern and topography: A tool for assessing potential water and soil losses in drylands, *Water Resour. Res.*, *44*, W10423, doi:10.1029/2007WR006367.

Meron, E., E. Gilad, J. von Hardenberg, M. Shachak, and Y. Zarmi (2004), Vegetation patterns along a rainfall gradient, *Chaos Solitons Fractals*, *19*(2), 367–376.

Michaelides, K., D. Lister, J. Wainwright, and A. J. Parsons (2009), Vegetation controls on small-scale runoff and erosion dynamics in a degrading dryland environment, *Hydrol. Processes*, *23*, 1617–1630, doi:10.1002/hyp.7293.

Moreno-de las Heras, M., J. M. Nicolau, L. Merino-Martin, and B. P. Wilcox (2010), Plot-scale effects on runoff and erosion along a slope degradation gradient, *Water Resour. Res.*, *46*, W04503, doi:10.1029/2009WR007875.

Moreno-de las Heras, M., P. M. Saco, G. R. Willgoose, and D. J. Tongway (2011a), Assessing landscape structure and pattern fragmentation in semiarid ecosystems using patch-size distributions, *Ecol. Appl.*, *21*(7), 2793–2805, doi:10.1890/10-2113.1.

Moreno-de las Heras, M., T. Espigares, L. Merino-Martín, and J. M. Nicolau (2011b), Water-related ecological impacts of rill erosion processes in Mediterranean-dry reclaimed slopes, *Catena*, *84*, 114–124.

Moreno-de las Heras M., P. M. Saco, G. R. Willgoose, and D. Tongway (2012), Variations in hydrological connectivity of Australian semiarid landscapes indicate abrupt changes in rainfall-use efficiency of vegetation, *J. Geophys. Res.*, *117*, G03009, doi:10.1029/2011JG001839.

National Research Council (2010), *Landscapes on the Edge: New Horizons for Research on Earth's Surface*, 180 pp., National Academies Press, Washington D.C.

Okin, G. S., A. J. Parsons, J. Wainwright, J. E. Herrick, B. T. Bestelmeyer, D. C. Peters, and E. L. Fredrickson (2009), Do changes in connectivity explain desertification?, *BioScience*, *59*, 237–244.

Puigdefábregas, J. (2005), The role of vegetation patterns in structuring runoff and sediment fluxes in drylands, *Earth Surf. Processes Landforms*, *30*, 133–147, doi:10.1002/esp.1181.

Puigdefábregas, J., and G. Sánchez (1996), Geomorphological implications of vegetation patchiness in semi-arid slopes, in *Advances in Hillslope Processes*, vol. 2, edited by M. Anderson and S. Brooks, pp. 1027–1060, Wiley, New York.

Puigdefábregas, J., A. Sol., L. Gutierrez, G. del Barrio, and M. Boer (1999), Scales and processes of water and sediment redistribution in drylands: Results from the Rambla Honda field site in SE Spain, *Earth Sci. Rev.*, *48*, 39–70.

Ravi, S., D. D. Breshears, T. E. Huxman, and P. D'Odorico (2010), Land degradation in drylands: Interactions among hydrologic–aeolian erosion and vegetation dynamics, *Geomorphology*, *116*(3–4), 236–245, doi:10.1016/j.geomorph.2009.11.023.

Reinhardt, L., D. Jerolmack, B. J. Cardinale, V. Vanacker, and J. Wright (2010), Dynamic interactions of life and its landscape: Feedbacks at the interface of geomorphology and ecology, *Earth Surf. Processes Landforms*, *35*, 78–101.

Rietkerk, M., M. C. Boerlijst, F. van Langevelde, R. HilleRisLambers, J. van de Koppel, L. Kumar, H. H. T. Prins, and A. M. de Roos (2002), Self-organization of vegetation in arid ecosystems, *Am. Nat.*, *160*(4), 524–530.

Rietkerk, M., S. C. Dekker, P. C. de Ruiter, and J. van de Koppel (2004), Self-organized patchiness and catastrophic shifts in ecosystems, *Science*, *305*(5692), 1926–1929.

Saco, P. M., and J. F. Rodriguez (2013), Modeling ecogeomorphic systems, in *Treatise on Geomorphology*, vol. 2, *Quantitative Modeling in Geomorphology*, edited by J. Shroder Jr. and A. C. W. Baas, Elsevier, San Diego, Calif., in press.

Saco, P. M., G. R. Willgoose, and G. R. Hancock (2007), Eco-geomorphology of banded vegetation patterns in arid and semi-arid regions, *Hydrol. Earth Syst. Sci.*, *11*, 1717–1730.

Scanlon, T. M., K. K. Caylor, S. A. Levin, and I. Rodríguez-Iturbe (2007), Positive feedbacks promote power-law clustering of Kalahari vegetation, *Nature*, *449*, 209–214, doi:10.1038/nature06060.

Sánchez, G., and J. Puigdefábregas (1994), Interactions of plant growth and sediment movement on slopes in a semi-arid environment, *Geomorphology*, *9*, 243–260.

Scholes, R. J., and S. R. Archer (1997), Tree-grass interactions in savannas, *Annu. Rev. Ecol. Syst.*, *28*, 517–544.

Slatyer, R. O. (1961), Methodology of a water balance study conducted on a desert woodland Acacia aneura community, *Arid Zone Res.*, *16*, 15–26.

Thompson, S. E., C. J. Harman, P. Heine, and G. G. Katul (2010), Vegetation-infiltration relationships across climatic and soil type gradients, *J. Geophys. Res.*, *115*, G02023, doi:10.1029/2009JG001134.

Tongway, D. J., and J. A. Ludwig (1990), Vegetation and soil patterning in semiarid mulga lands of Eastern Australia, *Aust. J. Ecol.*, *15*(1), 23–34.

Tongway, D. J., and J. A. Ludwig (2001), Theories on the origins, maintenance, dynamics, and functioning of banded landscapes, in *Banded Vegetation Patterning in Arid and Semiarid Environments: Ecological Processes and Consequences for Management, Ecolical Studies*, vol. 149, edited by D. J. Tongway, C. Valentin, and J. Seghieri, pp. 20–31, Springer, New York.

Turnbull, L., J. Wainwright, and R. E. Brazier (2008), A conceptual framework for understanding semi-arid land degradation: Ecohydrological interactions across multiple-space and time scales, *Ecohydrology*, *1*, 23–34.

Valentin, C., J.-M. D'Herbes, and J. Poesen (1999), Soil and water components of banded vegetation patterns, *Catena*, *37*(1–2), 1–24.

von Hardenberg, J., E. Meron, M. Shachak, and Y. Zarmi (2001), Diversity of vegetation patterns and desertification, *Physical Review Letters*, *87*(19), Article 198101.

Wainwright, J., A. J. Parsons, W. H. Schlesinger, and A. D. Abrahams (2002), Hydrology-vegetation interactions in areas of discontinuous flow on a semi-arid bajada, southern New Mexico, *J. Arid Environ.*, *51*(3), 319–338, doi:10.1006/jare.2002.0970.

Wheaton, J. M., C. Gibbins, J. Wainwright, L. Larsen, and B. Mcelroy (2011), Geomorphology preface: Multiscale feedbacks in ecogeomorphology, *Geomorphology*, *126*(3–4), 265–268, doi:10.1016/j.geomorph.2011.01.002.

Wilcox, B. P., D. D. Breshears, and C. D. Allen (2003), Ecohydrology of a resource-conserving semiarid woodland: Effects of scale and disturbance, *Ecol. Monogr.*, *73*(2), 223–239.

Willgoose, G. R. (2005), User Manual for Siberia (Version 8.30) [Available at http://www.telluricresearch.com/siberia-homepage.html, accessed date 02/01/13].

Willgoose, G. R., and S. Riley (1998), The long-term stability of engineered landforms of the Ranger Uranium Mine, Northern Territory, Australia: Application of a catchment evolution model, *Earth Surf. Processes Landforms*, *23*, 237–259.

Willgoose, G. R., R. L. Bras, and I. Rodriguez-Iturbe (1991), A physically based coupled network growth and hillslope evolution model: 1. Theory, *Water Resour. Res.*, *27*(7), 1671–1684.

Yetemen, O., E. Istanbulluoglu, and E. R. Vivoni (2010), The implications of geology, soils, and vegetation on landscape morphology: Inferences from semi-arid basins with complex vegetation patterns in central New Mexico, USA, *Geomorphology*, *116*(3–4), 246–263, doi:10.1016/j.geomorph.2009.11.026.

Zhang, H. (1994), Organic matter incorporation affects mechanical properties of soil aggregates, *Soil Tillage Res.*, *31*, 263–275.